

# Dealloyed PtNi-Core–Shell Nanocatalysts Enable Significant Lowering of Pt Electrode Content in Direct Methanol Fuel Cells

Andreas Glüsen,<sup>\*,†</sup> Fabio Dionigi,<sup>‡</sup> Paul Paciok,<sup>§</sup> Marc Heggen,<sup>§</sup> Martin Müller,<sup>†</sup> Lin Gan,<sup>||</sup> Peter Strasser,<sup>‡</sup> Rafal E. Dunin-Borkowski,<sup>§</sup> and Detlef Stolten<sup>†,⊥</sup>

<sup>†</sup>Institute of Energy and Climate Research IEK-3: Electrochemical Process Engineering, Forschungszentrum Jülich, 52425 Jülich, Germany

<sup>‡</sup>The Electrochemical Energy, Catalysis and Materials Group, Department of Chemistry, Technical University Berlin, 10623 Berlin, Germany

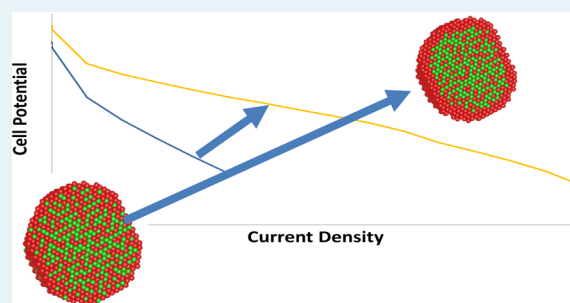
<sup>§</sup>Ernst-Ruska Centre for Microscopy and Spectroscopy with Electrons, Forschungszentrum Jülich GmbH, 52425 Jülich, Germany

<sup>||</sup>Division of Energy and Environment, Graduate School at Shenzhen, Tsinghua University, Shenzhen 518055, China

<sup>⊥</sup>Chair for Fuel Cells, RWTH Aachen University, 52072 Aachen, Germany

**ABSTRACT:** Direct methanol fuel cells (DMFCs) have the major advantage of the high energy density of the methanol (4.33 kWh/l) they use as a liquid fuel, although their costs remain too high due to the high quantity of Pt needed as a catalyst for oxygen reduction in the presence of methanol. Pt–Ni core–shell catalysts are promising candidates for improved oxygen reduction kinetics as shown in hydrogen fuel cells. The novelty in this work is due to the fact that we studied these catalysts in DMFC cathodes where oxygen must be reduced and membrane-permeating methanol oxidized at the same time. In spite of many attempts to overcome these problems, high amounts of Pt are still required for DMFC cathodes. During measurements over more than 3000 operating hours, the performance of the core–shell catalysts increased so substantially that a similar performance to that obtained with five times the amount of commercial platinum catalyst was achieved. While catalyst degradation has been thoroughly studied before, we showed here that these catalysts exhibit a self-protection mechanism in the DMFC cathode environment and prolonged operation is actually beneficial for performance and further stability due to the formation of a distinct Pt-rich shell on a PtNi core. The catalyst was analyzed by transition electron microscopy to show how the catalyst structure had changed during activation of the core–shell catalyst.

**KEYWORDS:** direct methanol fuel cell, Pt–Ni core–shell nanoparticles, oxygen reduction reaction, scanning transmission electron microscopy, structural change



## 1. INTRODUCTION

In recent years, direct methanol fuel cells (DMFCs) have been developed to a state of technological readiness at which their application is possible in fields where the high energy density of liquid methanol (4.33 kWh/l) is especially advantageous. These fields of interest include, in particular, material handling,<sup>1,2</sup> uninterruptable power supply (UPS),<sup>3</sup> auxiliary power units and portable applications,<sup>4</sup> as well as applications in remote areas in the power range of several watts<sup>4</sup> to a few kW.<sup>5</sup> The costs of DMFC systems, however, are still relatively high, and therefore, the systems presently on the market are fairly limited. The main component that accounts for the high costs is the membrane electrode assembly (MEA), owing to the large amount of platinum used as a catalyst.<sup>5</sup> Therefore, it would be desirable to have a catalyst with increased activity in comparison to pure platinum so that a much smaller amount of platinum would be sufficient to achieve the same performance.

In DMFCs, the amount of platinum required is higher than in hydrogen fuel cells because the carbon–oxygen bond in

methanol is not easy to break.<sup>6</sup> This is not only relevant for the anode, where the methanol oxidation reaction is the main reaction,<sup>7,8</sup> but also for the cathode. There, methanol permeating from the anode is adsorbed onto the catalyst and must be oxidized to avoid poisoning of the catalyst and allow the oxygen reduction reaction (ORR) to take place. Therefore, a good cathode catalyst must be able to oxidize methanol and reduce oxygen at the same time. In Pt-based cathode catalysts, permeating methanol is completely adsorbed and oxidized at the cathode. The amount of methanol oxidized at the cathode is therefore determined by the amount of methanol permeating to the cathode. A higher reaction rate for methanol oxidation at the cathode catalyst therefore means that a smaller portion of the cathode catalyst is used for methanol oxidation and more is available for oxygen reduction. The only alternative

**Received:** December 6, 2018

**Revised:** February 19, 2019

**Published:** March 20, 2019

would be a methanol tolerant cathode catalyst that does not adsorb permeating methanol. Catalyst types examined in the literature include Pt-based alloy catalysts,<sup>9–11</sup> catalysts based on other platinum group metals (PGM) like Ru<sup>12</sup> and Pd,<sup>13</sup> and PGM-free catalysts.<sup>14,15</sup> While Pt-based catalysts always show methanol oxidation and oxygen reduction, they can be optimized to increase oxygen reduction and decrease methanol oxidation. Ru and Pd-based catalysts can be designed so that they do not oxidize methanol, but larger amounts of the expensive PGMs are needed. The performance of PGM-free catalysts is still limited. In a recent review, it was shown that when operated with air at the cathode, the Pt efficiency in the resulting DMFCs is below 20 W/g Pt, less than for DMFCs with commercial Pt cathodes. This is due to low performance, and Pt is still required at the anode. A problem with cathodes that do not oxidize methanol is that toxic methanol vapor can be emitted from the cathode exhaust, excluding indoor use of such fuel cells. Methanol permeation could also be reduced by using an anode or a membrane<sup>16–18</sup> that does not allow methanol to pass easily to the cathode or by removing permeating methanol before it reaches the cathode.<sup>19</sup> Even then, however, a certain amount of methanol will pass to the cathode, and a good cathode is still required. To alleviate this problem, DMFC systems are operated with dilute aqueous methanol solution in a concentration of usually between 0.4 and 1.0 molar.<sup>5</sup> This solution is circulated through the cells and replenished from a tank of pure methanol according to the amount of methanol consumed in the fuel cell to maintain a constant concentration.

At present, the standard cathode catalysts are Pt nanoparticles supported on high surface area carbon. It has been shown that the catalytic activity of Pt surfaces depends on the heat of adsorption of oxygen<sup>20</sup> on the surface, which can be controlled by changing the position of the Pt *d*-band center.<sup>21</sup> A maximum of activity is observed where both the adsorption and oxidation of oxygen occur rapidly. Deviations from this optimum lead to either less adsorption of oxygen on the surface or slower oxidation and desorption of the products. Pt alloys with different metals were used to fine-tune the heat of adsorption of oxygen on the surface. For example, alloys of Pt with Sn,<sup>22</sup> Ni,<sup>23</sup> Co,<sup>24</sup> and other transition metals were used, and higher catalytic activity toward the ORR was obtained in several cases.<sup>20,25</sup> Pt–Ni–P catalysts have been shown to be effective in methanol oxidation as well.<sup>26</sup> The stability of these alloys was, however, not always adequate for application in fuel cells.

A variation in the lattice constant of the Pt surface can also be used to tune the heat of adsorption of oxygen on the surface. By applying a Pt coating on top of another metal with a similar but not identical lattice constant, a change in the lattice constant can be obtained. Core–shell nanoparticles were developed to make use of this principle and, at the same time, have a high active surface in relation to their weight. Different structures of nanoparticles have been used: they can be spherical<sup>27</sup> or octahedral<sup>28–30</sup> or have a different structure altogether.<sup>31</sup> For the synthesis of core–shell particles, either a less noble core particle can be coated with the active material<sup>32–34</sup> or the less noble component of an alloy particle can be removed from the surface by annealing<sup>21,24,35,36</sup> or leaching<sup>37,38</sup> so that a Pt shell or Pt-rich alloy shell is formed. It was shown that the compressive lattice strain in a Pt shell formed on a Pt-alloy core was most favorable for a high catalytic activity.<sup>39</sup> For optimal catalytic activity, it was found

that the Pt shell thickness of a core–shell particle is significant and that catalytic activity is highest for a Pt shell thickness of 2–5 atomic layers.<sup>40</sup> Thus, a detailed understanding of the fine structure of core–shell catalysts is important.

For long lasting fuel cells, the catalyst durability is crucial. For material handling applications, an operating time of 20 000 h<sup>5</sup> is required, while standby time is more relevant for UPS applications.<sup>3</sup> Here, a standby time of 10 years is required, while the system must withstand frequent start-up and shut-down procedures. A minimum of 140 cycles is necessary over a 10-year lifetime, assuming monthly tests of function and two power outages per year, where the UPS system has to provide power. While nanoparticles containing non-noble metals can be expected to be unstable under fuel cell cathode conditions, it was shown in the literature that less noble core particles protected by a platinum shell can be more stable than pure Pt nanoparticles.<sup>41</sup>

DMFCs systems are not heated externally, and therefore, the temperature where the system is in thermal equilibrium will be reached after a while.<sup>2</sup> The DMFC is heated by having a cell voltage below the voltage corresponding to the heating value of methanol: the rest is converted into heat and methanol permeation, where methanol permeating to the cathode is oxidized without generating current. The cooling is mainly due to the evaporation of water at the cathode, which must be limited by using a limited cathodic air flow.<sup>42</sup> The aim is to operate the DMFC at a thermal equilibrium at approximately 70 °C with a methanol concentration as low as possible to achieve a high current generating efficiency. Therefore, a suitable catalyst must be capable of operating at limited air flow without a loss in cell potential.

In this work, we used a catalyst which had already shown good performance in the cathode of hydrogen fuel cells and studied it under the conditions of a DMFC cathode, where oxygen and, due to permeation, methanol are present at the same time and oxygen reduction reaction needs to be able to take place efficiently in the presence of methanol and its intermediate oxidation products like carbonyl species. Methanol adsorbs quickly onto the catalyst, and if it is not or only partly oxidized, it poisons the cathode for ORR reaction. An efficient cathode catalyst for DMFCs must therefore be able to oxidize methanol to free catalyst surface for the ORR reaction.<sup>43</sup>

Degradation mechanisms in DMFC cathodes are different from those in hydrogen fuel cell cathodes. Due to permeation, the cathode potential in DMFCs is lower, so oxidative corrosion of Pt is less relevant.<sup>44</sup> However, the permeation of water, present in abundance at the anode of DMFCs, leads to liquid water in the cathode in many operating states, which allows dissolution of oxidized species. In summary, catalyst is not oxidized easily, but once oxidized, it can be removed easily from the electrode. So, we can expect that Pt is very stable in DMFC cathodes, while less noble metals, in our work Ni, are removed more easily from DMFC cathodes than from cathodes in hydrogen fuel cells.

## 2. MATERIALS AND METHODS

**2.1. Catalysts.** The core–shell catalysts were PtNi<sub>3</sub> catalysts supported on high surface area carbon, as described previously.<sup>27</sup> The core–shell catalysts were dealloyed by treating in 0.5 molar sulfuric acid at 70 °C for 24 h. The catalyst powder was then filtered and washed three times by suspending it in deionized water and filtering it again. A

commercial HiSpec 3000 by Johnson Matthey (20% Pt on Vulcan XC72) was used as received for comparison.

**2.2. Membrane Electrode Assemblies (MEAs).** MEAs were made by dispersing the catalyst and coating it onto gas diffusion layers (GDLs) to form gas diffusion electrodes (GDEs), which were then hot-pressed with the membrane to form the MEA.

The cathode catalyst ink was made by wetting 150 mg of catalyst with 150 mg of water to avoid autoignition. Then, a mixture of 1.29 mL of 1-propanol and 0.43 mL of 2-propanol was added, and the mixture was homogenized by sonication. Nafion solution LQ1115 (Ion Power) (728 mg) was added, and the mixture was sonicated again.

The ink was then spread onto the GDL by knife-coating with a distance of 50  $\mu\text{m}$  (core-shell catalyst and low loading of the HiSpec 3000) or 300  $\mu\text{m}$  (high loading of the HiSpec 3000).

Anodes were made by a similar process using a commercial PtRu-based catalyst (HiSpec 12 100, Johnson Matthey). A loading of 3.2  $\text{mg}/\text{cm}^2$  of PtRu was obtained.

Carbon felt materials type H2315 CX312 (cathode) and H2315 I6 (anode), both from FFCCT (Freudenberg Fuel Cell Component Technologies), were used as GDLs.

The anode and cathode were hot-pressed with a Nafion 115 (Dupont) membrane at 130  $^{\circ}\text{C}$  and 0.5  $\text{kN}/\text{cm}^2$  for 3 min.

**2.3. DMFC Testing.** The MEAs, with an active area of  $42 \times 42 \text{ mm}^2$ , were mounted into a custom-built test cell with 200  $\mu\text{m}$  PTFE flat gaskets on both the anode and the cathode sides. Flow-field plates with a machined checkerboard flow-field made from polymer-bound graphite material (Sigracet from SGL carbon) were used. The channel dimensions were 1 mm wide, 1 mm deep, and 1 mm distant between the channels. The flow field plates were mounted between stainless steel end-plates that were heated with heating cartridges and tightened with eight nuts (M6) and bolts around the perimeter to a torque of 5 N m.

The cells were operated on custom-built test-rigs. On the anode side, methanol solutions of different concentrations (0.5 molar, 0.75 molar and 1 molar) were pumped by a peristaltic pump through a preheating cell into the test cell at a flow rate of 0.22  $\text{mL}/(\text{cm}^2\cdot\text{min})$ . The preheating cell and test cell were set to 70  $^{\circ}\text{C}$ . On the cathode side, dry compressed air was let into the cell by a mass-flow controller with no back-pressure applied. The test-rigs were controlled by in-house software based on Lab View. To protect the cells from corrosion, the cell voltage was monitored, and when it fell below 0.1 V, the measurement at these conditions was stopped, and the program jumped to the next step without a current load.

To activate and study the cells, different operating procedures were utilized, as listed in Table 1. The activation procedure consists of five sets of three current-potential curves recorded at high air flow rates of 37  $\text{mNL}/(\text{cm}^2\cdot\text{min})$ . Between sets, the test cell was again cooled to room temperature for 2 h and heated to 70  $^{\circ}\text{C}$ . After that, measurements with a constant current density of 0.06  $\text{A}/\text{cm}^2$  and varying air-flow rates of 3  $\text{mNL}/(\text{cm}^2\cdot\text{min})$  to 20  $\text{mNL}/(\text{cm}^2\cdot\text{min})$  were performed with different methanol concentrations. Then, sets of three current-potential curves as described above were obtained at different methanol concentrations. The second current-potential curve for each concentration was used in the results. Afterward, measurements at a constant current density of 0.1  $\text{A}/\text{cm}^2$  and varying air flow rates were conducted with different methanol

**Table 1. Measurement Routines Performed on the MEAs**

procedure	duration (h)	cumulative duration (h)	$U-i$ curve taken @ (h)
activation 1	95	95	37
start-stop	190	285	
activation 2	95	380	322
start-stop	233	613	
activation 3	95	708	650
start-stop	840	1548	
activation 4	95	1643	1585
activation 5	95	1738	1680
activation 6	95	1833	1775
start-stop	598	2431	
activation 7	95	2526	2468
start-stop	69	2595	
continuous operation	1051	3646	
activation 8	95	3741	3683
activation 9	95	3836	3778

concentrations. These were used in the results as well. Current potential curves and measurements at constant current density were then repeated with a different order of methanol concentrations to exclude the influence of the previous methanol concentration.

Start-stop cycles were performed in a different test rig, where the three cells were electrically connected in series so they had the same current density at all times, with the minimum potential for one cell set to 0.05 V. The cells were gradually heated with an air flow rate of 6.5  $\text{mNL}/(\text{cm}^2\cdot\text{min})$  and, at a temperature of 33  $^{\circ}\text{C}$ , an initial load of 0.01  $\text{A}/\text{cm}^2$  was applied and increased in steps of 0.01  $\text{A}/\text{cm}^2$  until the final load of 0.1  $\text{A}/\text{cm}^2$  was reached at a temperature of 50  $^{\circ}\text{C}$ . The air flow rate was increased to 15  $\text{mNL}/(\text{cm}^2\cdot\text{min})$ , and heating continued until 60  $^{\circ}\text{C}$  was reached. Then operation at 60  $^{\circ}\text{C}$  was continued for 3 h. Then, the load, air flow, and methanol flow were switched off, and the cell was left to cool to room temperature. Twelve hours later, the next operating cycle was started. To monitor the state of the cells, a current-potential curve was included once per week. This procedure was the result of a previous project aiming at a quick start-up without additional degradation.

Continuous operation was performed in the same test rig as the start-stop cycles. The cells were operated continuously for 30 min at 0.1  $\text{A}/\text{cm}^2$  and 15  $\text{mNL}/(\text{cm}^2\cdot\text{min})$  air flow rate; then, current flow and air flow were interrupted for a few seconds to remove reversible degradation, and continuous operation was resumed. Once every 100 h, a set of current-potential curves was recorded to monitor the state of the cells.

**2.4. Analysis of Catalysts.** After fuel cell operation, some catalyst was scratched off from the membrane for analysis. The same was carried out with an unused electrode for comparison.

Scanning transmission electron microscopy (STEM) was performed using a FEI Titan 80-200 (ChemSTEM) electron microscope operated at 80 kV and equipped with a spherical aberration (Cs) probe corrector (CEOS GmbH) and high angle annular dark field (HAADF) detector. A probe semi angle of 17.7 mrad and a detector inner collection semi angle of 88 mrad were used. Compositional maps were obtained with energy-dispersive X-ray spectroscopy (EDX) using four large-solid-angle symmetrical Si drift detectors. For the EDX analysis, Pt L and Ni K peaks were used.

### 3. RESULTS AND DISCUSSION

The PtNi core-shell catalyst (25% PtNi on carbon black) was used to make a DMFC cathode and compared to cathodes made with the commercial catalyst HiSpec 3000 (20% Pt on carbon black). Catalyst loading was  $89 \mu\text{g}/\text{cm}^2$  Pt for the core-shell-catalyst and 86 and  $410 \mu\text{g}/\text{cm}^2$  Pt for the commercial catalyst (similar loading to the core-shell and 5-fold loading). All of these loadings are significantly lower than those of cathodes on commercial DMFC-MEAs, which have about  $1\text{--}2 \text{ mg}/\text{cm}^2$  of Pt<sup>1,45</sup> and show an even higher level of performance as well as homemade MEAs with the same cathode loading. Therefore, it can be assumed that the effects presented here are actually due to the cathode's properties and are not limited by the anode performance or membrane resistance.

At the beginning of life, it was found that the MEA with core-shell cathode performed poorly, as did the MEA with the low loading of the commercial catalyst (Figure 1a). After

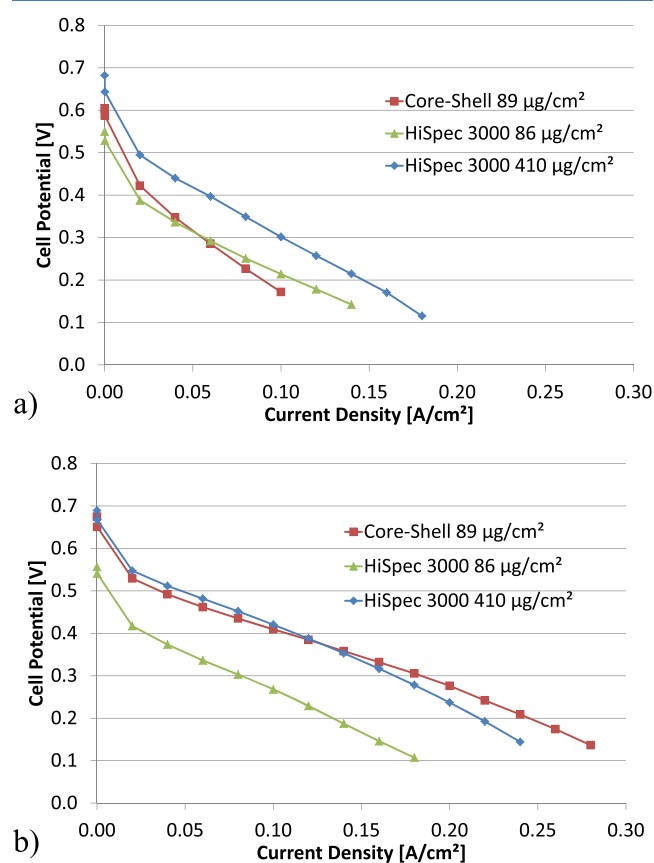


**Figure 1.** (a) Current potential curves after 37 h and (b) after 1775 h; 0.75 M methanol solution at  $0.22 \text{ mL}/(\text{cm}^2\cdot\text{min})$ , air at  $37 \text{ mL}/(\text{cm}^2\cdot\text{min})$  and ambient pressure,  $70^\circ\text{C}$ .

several activation procedures and start-stop cycling over a total of 1775 operating hours (see Table 1), however, the MEA with the core-shell cathode had significantly improved and performed similarly to the MEA with the 5-fold loading of the commercial catalyst (Figure 1b). Through analysis of the current-potential curves in more detail, a small increase in cell potential at zero and low current densities can be detected ( $0.071 \text{ V}$  at  $0 \text{ A}/\text{cm}^2$ ), while the increase at higher current densities is especially large ( $0.237 \text{ V}$  at  $0.1 \text{ A}/\text{cm}^2$ ). The comparison of the cell voltages at the highest current densities

shows an inferior performance of the core-shell MEA at BoL, but after 1775 operation hours, the low loaded core-shell MEA outperforms the MEA with 5-fold platinum loading with a commercial catalyst.

In general, the open cell voltage in direct methanol fuel cells is low compared to that in hydrogen fuel cells. This is caused by the mixed potential at the cathode of oxygen reduction and methanol oxidation due to the permeation of methanol from the anode to the cathode. The cathode potential therefore depends on the relative amounts of methanol and oxygen reacting at the cathode.<sup>46</sup> Through use of the same operating conditions, the amounts of methanol and oxygen present at the cathode are the same. A change in open cell potential is therefore caused by a change in the relative turnover rates of the ORR and MOR. In contrast, the highest current density that can be achieved is due to the active surface area and exchange current density on the catalytic sites. When comparing the performance of the core-shell cathode at 37 and 1775 h (Figure 2a), it is obvious that the highest current density increases significantly, while the potential at zero current only increases a bit. A small increase in the open cell potential and a larger increase of the potential under load might therefore indicate a significantly increased turnover rate, while the relationship of turnover rates for oxygen reduction and methanol oxidation does not change significantly. In DMFC operation, the ohmic resistance is not as important as that in hydrogen fuel cells. The ohmic resistance in a DMFC MEA is generally between  $0.2$  and  $0.3 \Omega\text{cm}^2$  for MEAs containing Nafion 115 and an operating temperature of  $70^\circ\text{C}$ .<sup>19</sup> The slope of the current-potential curve, however, is more than  $1 (\text{V}/\text{A})\text{cm}^2$  for all curves shown in this paper.

The development of the three MEAs over time was very different. While the core-shell MEA improved continuously (Figure 2a), the MEA with the low loading of commercial catalyst was only negligibly improved only at the beginning and then started to degrade (Figure 2b), while the MEA with the high loading of commercial catalyst improved over time, but much less so than the core-shell MEA (Figure 2c). The gain in cell potential from 37 to 1775 h was  $0.099 \text{ V}$  for the MEA with the high loading of commercial catalyst vs  $0.237 \text{ V}$  for the MEA with the core-shell catalyst. The initial activation of the MEA is generally due to humidification of the membrane and the ionomer in the catalyst layers. Also, a deactivating surface on the catalyst may need to be removed.<sup>47</sup> These processes generally take place within 100 to a few hundreds of operating hours. The speed of these processes can depend on the state of the membrane and the Nafion content in the catalyst layers.<sup>48</sup> The fact that the cell potential of the MEA with the core-shell catalyst on the cathode increases significantly, even beyond 650 operating hours, indicates that additional processes take place that are much slower.

When operating the DMFC with reduced air flow, which is important for system operation,<sup>2</sup> the core-shell catalyst demonstrated a superior performance compared to that of the commercial catalyst, even at a fivefold higher loading (Figure 3). While the cell potential at  $0.1 \text{ A}/\text{cm}^2$  after 1775 operating hours in the current-potential curves recorded at an air flow rate of  $37 \text{ mL}/(\text{cm}^2\cdot\text{min})$  are almost identical for the higher loading of commercial catalyst and core-shell catalyst, the potential of the MEA with the commercial catalyst decreases significantly when the air flow rate is reduced to  $20 \text{ mL}/(\text{cm}^2\cdot\text{min})$  and less. The cell potential of the MEA with the core-shell catalyst remains almost constant up to an air

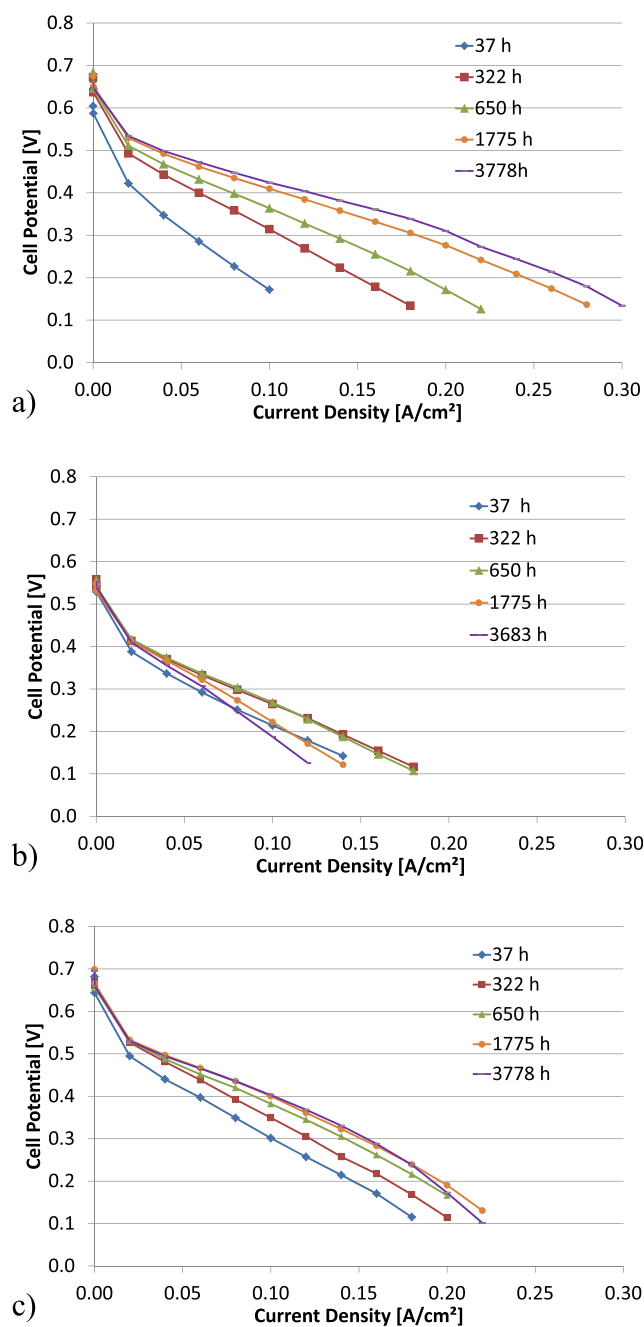


**Figure 2.** (a) Development of current–potential curves for MEAs with  $89 \mu\text{g}/\text{cm}^2$  core–shell catalyst, (b)  $86 \mu\text{g}/\text{cm}^2$  HiSpec 3000, and (c)  $410 \mu\text{g}/\text{cm}^2$  HiSpec 3000; 0.75 M methanol solution at  $0.22 \text{ mL}/(\text{cm}^2\text{-min})$ , air at  $37 \text{ mL}/(\text{cm}^2\text{-min})$  and ambient pressure,  $70 \text{ }^\circ\text{C}$ .

flow rate of 10 to  $15 \text{ mL}/(\text{cm}^2\text{-min})$  depending on the methanol concentration, and only below that can a significant decay of cell potential be observed. In general, the decay of cell potential with decreasing air flow is more significant for higher methanol concentrations, as these lead to increased methanol permeation and a higher contribution of methanol oxidation to the mixed potential at the cathode. The effect of methanol concentration on cell potential is smaller for the core–shell catalyst. This might indicate that methanol is oxidized more quickly on the core–shell catalyst than on the commercial catalyst. However, an independent measurement of methanol oxidation and oxygen reduction is not possible in the DMFC. In a full DMFC system, air flow rates in the range of 10–15

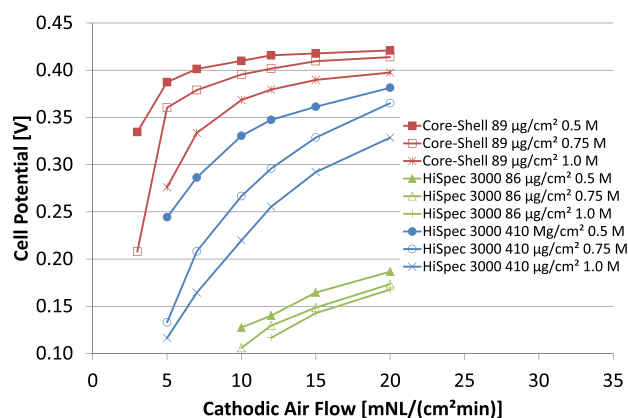


**Figure 3.** Dependence of cell potential at  $0.1 \text{ A}/\text{cm}^2$  on cathodic air flow after 1775 operating hours; 0.5, 0.75, and 1 M methanol solution at  $0.22 \text{ mL}/(\text{cm}^2\text{-min})$ , air at ambient pressure,  $70 \text{ }^\circ\text{C}$ .

$\text{mNL}/(\text{cm}^2\text{-min})$  should be utilized to keep the cell at a favorable operating temperature. Based on the presented results, while the operation of a DMFC at low air flow rates is feasible with the core–shell catalyst even at low cathode loadings, the usage of the commercial catalyst induces significant losses in cell performance at both loadings. A possible explanation for this has been given by Greeley.<sup>20</sup> Due to the lower oxygen adsorption energy, the active sites are more quickly liberated from adsorbed intermediate species. Therefore, more free catalytic sites are available for the adsorption of the next oxygen molecule.

When the DMFC was operated with different methanol concentrations resulting in different amounts of methanol permeating to the cathode, the effect of the concentration was similar in all cases. This shows that the tolerance of methanol is similar for the commercial and core–shell catalyst (Figure 4). A higher methanol concentration in the concentration range considered here leads to better performance of the anode, while a lower methanol concentration leads to better performance of the cathode. Generally, the effect of the methanol concentration on the anode is more significant at high current densities, while the effect of the methanol concentration on the cathode is similar for all current densities. Therefore, the optimal methanol concentration increases with increased current density.

For durability testing, an intermittent operation consisting of 140 start–stop cycles<sup>3</sup> within 70 days and a continuous operation of 1000 h was performed. During intermittent operation, the core–shell MEA improved, while the cell voltage of the MEA with a high loading of commercial catalysts remained constant and the MEA with a low loading of commercial catalyst degraded (Figure 5a). The improvement in the performance over a long period shows that a slow process is responsible for this. This may be caused by a dealloying or restructuring process of the catalyst.<sup>30</sup> Far below the melting point of the metals, such a change in structure is expected to be extremely slow.

During continuous operation, the performance of all the MEAs degraded slightly. The trend in degradation was core–shell < high-loading commercial < low-loading commercial (Figure 5b). While commercial catalysts already show good stability, allowing the design of a DMFC system that can be operated for 20 000 h,<sup>5</sup> the stability of the core–shell catalyst appears to be even better. It is therefore a promising candidate

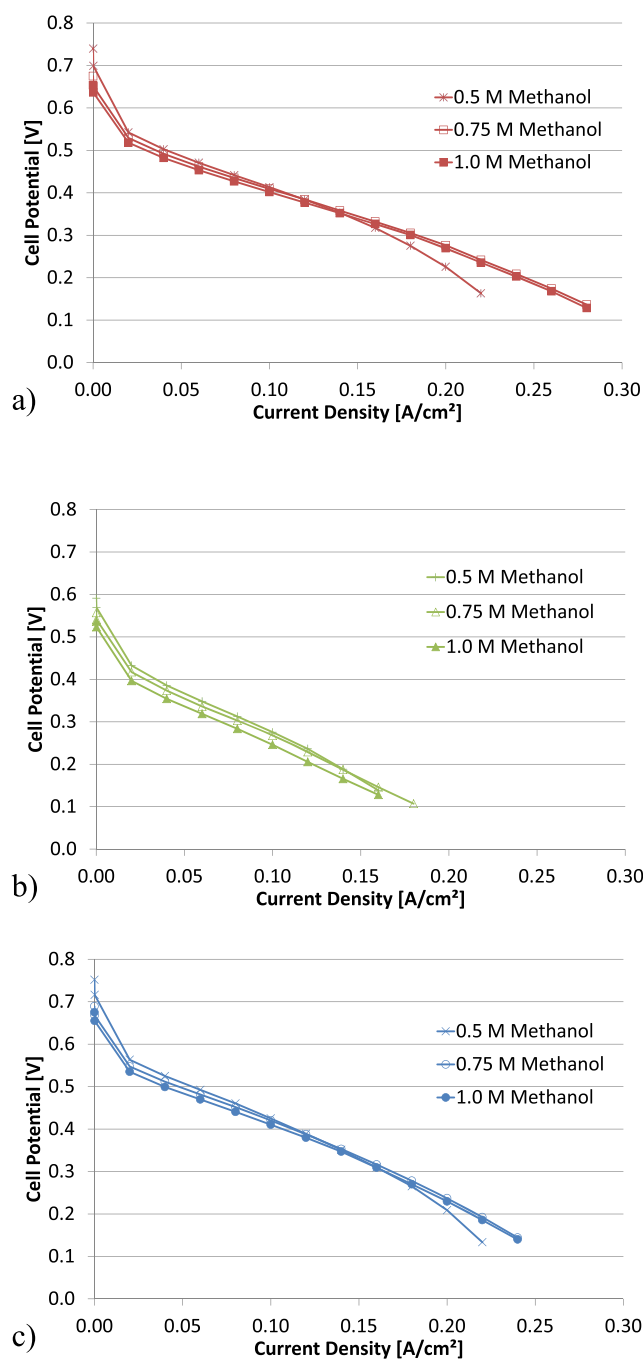


**Figure 4.** (a) Current potential curves at different methanol concentrations for MEAs with  $89 \mu\text{g}/\text{cm}^2$  core-shell catalyst, (b)  $86 \mu\text{g}/\text{cm}^2$  HiSpec 3000, and (c)  $410 \mu\text{g}/\text{cm}^2$  HiSpec 3000. Methanol solution at  $0.22 \text{ mL}/(\text{cm}^2\cdot\text{min})$ , air at  $37 \text{ mL}/(\text{cm}^2\cdot\text{min})$  and ambient pressure,  $70 \text{ }^\circ\text{C}$ .

for future DMFCs, allowing not only the use of less of the costly platinum metal but also increasing the long-term stability, leading to DMFC systems that can be operated for extended periods.

Before and after the electrochemical experiments, the catalyst was analyzed by STEM. Figure 6 shows representative HAADF images before and after the fuel cell test and the corresponding particle size distributions. After the acidic activation procedure,<sup>31</sup> the average particle diameter is  $6 \pm 1.7 \text{ nm}$ . The intermittent operation, simulated by 140 start-stop cycles and continuous operation for 1000 h, led to a

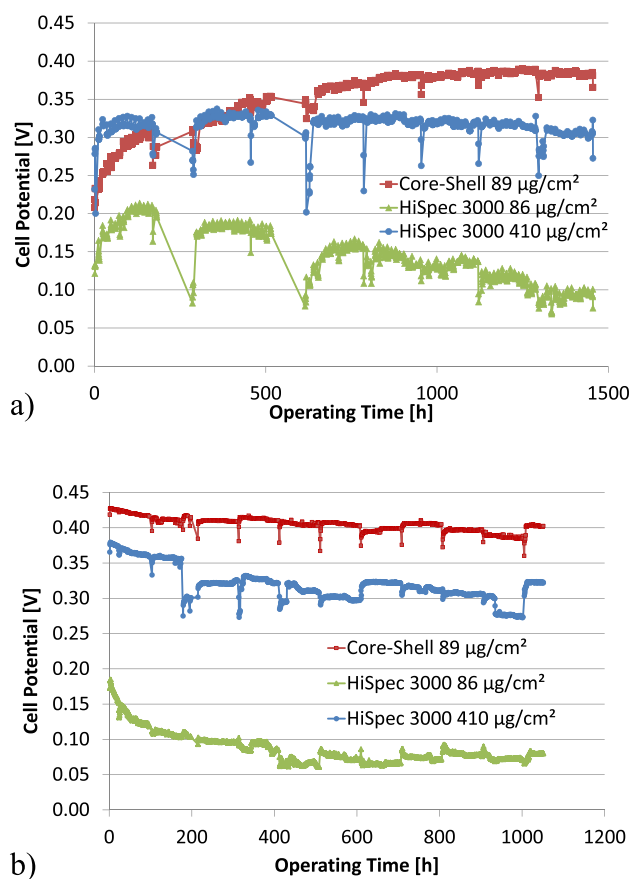


**Figure 5.** (a) Development of cell potential over time during start-stop cycling at  $60 \text{ }^\circ\text{C}$  and (b) during continuous operation at  $70 \text{ }^\circ\text{C}$ ;  $0.75 \text{ M}$  methanol solution at  $0.22 \text{ mL}/(\text{cm}^2\cdot\text{min})$ , air at  $15 \text{ mL}/(\text{cm}^2\cdot\text{min})$  and ambient pressure,  $0.1 \text{ A}/\text{cm}^2$ .

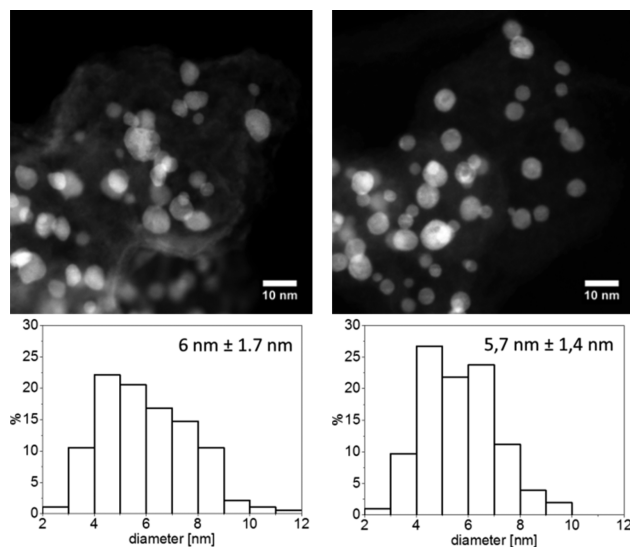


**Figure 6.** Representative HAADF images and particle size distributions of the PtNi-based catalyst before (left) and after (right) electrochemical aging.

decrease in the average particle diameter to  $5.7 \pm 1.4 \text{ nm}$ . Furthermore, the amount of particles with a diameter  $>7 \text{ nm}$  declined significantly, which can be attributed to a loss of Ni atoms.<sup>27</sup> The spherical morphology of the particles was also preserved.

The effect of the electrochemical experiment on the elemental composition of the particles was investigated by STEM-EDX. EDX maps and corresponding HAADF-STEM images of representative particles before and after the durability test are shown in Figure 7. The average platinum content of the analyzed particles before and after the durability tests was  $54 \pm 3$  atom %<sub>Pt</sub> and  $73 \pm 5$  atom %<sub>Pt</sub>, respectively (see Table 2).

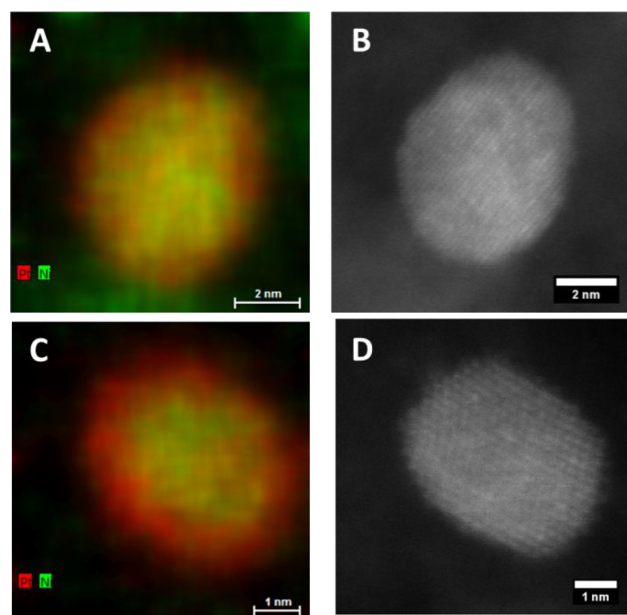


**Figure 7.** EDX maps (left) and corresponding HAADF-STEM images (right) of representative particles before (top) and after (bottom) the durability test.

**Table 2. Composition and Size of Core–Shell Particles from TEM Analysis**

	pristine electrode	electrode after operation
average Pt atom %	53.7	73.1
std dev Pt atom %	3.0	5.4
no. particles	7	11
average diameter (nm)	6.0	5.7
std dev diameter (nm)	1.7	1.4

Due to the potential cycling and operation for 1000 h, a dissolution of the nickel occurred, leading to the formation of a distinct platinum shell. The platinum concentration within the shell was  $92.6 \pm 1.4$  atom %<sub>Pt</sub>, while the core remained Ni-rich. Thus, the formation of a platinum-rich shell prevents the further nickel dissolution of the Ni-rich core. An analysis of the shell's thickness reveals values in the range of  $0.7 \pm 0.17$  nm. Based on the lattice spacing of Pt (111), the shell has the approximate thickness of three atom layers of platinum, the thickness that was previously found to be especially advantageous for oxygen reduction activity.<sup>40</sup>

Figure 8 shows a model of the core–shell structure of the catalyst before (left) and after (right) the electrochemical measurement. The change appears to be due to nickel leaching from the core, leading to a reduced particle diameter and thicker, Pt-rich shell. As indicated by the speed of the change in performance, it is expected that the leaching is quicker at the

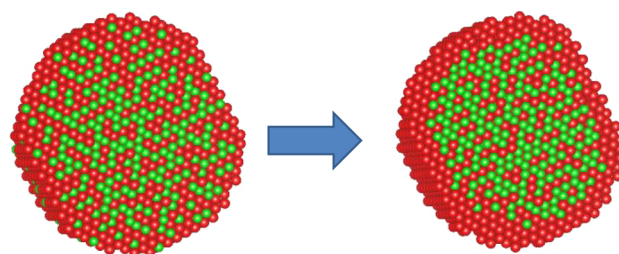


**Figure 8.** Model of the core–shell structure of the catalyst before (left) and after (right) electrochemical measurement. The change appears to be due to nickel (green) leaching from the core, leading to a reduced particle diameter and thicker, Pt-rich (red) shell. 3D models were represented using the VESTA program.<sup>49</sup>

beginning and then slows or even comes to a halt as the thicker Pt shell impairs access to the nickel-rich core.

#### 4. CONCLUSIONS

In this paper, a PtNi core–shell catalyst with an exceptionally high performance in the cathode of a DMFC is analyzed. The full potential of the catalyst was achieved only after more than 1000 operating hours under different operating conditions, and the change in structure that led to the high performance was characterized. While the core–shell catalyst initially only has a thin, Pt-rich shell and its performance is similar to the same amount of commercial Pt catalyst, during operation, a distinct Pt-rich shell develops and reaches a thickness of 0.7 nm, which is about the thickness of three layers of Pt atoms. This structure is connected to increased performance, similar to a cathode with five times the amount of commercial Pt catalyst at high air flow rates.

At reduced air flow rates, the performance of the core–shell catalyst is even better than that of five times the amount of commercial Pt catalyst, allowing operation at air flow rates that are relevant to DMFC systems without a loss of cell voltage.

During the measurements, spanning a total operating time of 3800 h, no decay of performance was observed, and so robust durability of the core–shell catalyst can be assumed. Due to these results, we concluded that Ni is necessary in the core and detrimental in the shell for both activity and stability.

The relatively long time taken to reach the full performance, however, is not desirable for application. Future catalyst designs will benefit from the results presented here because they identify what kind of structure a PtNi core–shell catalyst should have to show good performance and high durability at low Pt-loading. It would be necessary to find a way to make the catalyst with this structure so that optimum performance can be achieved following a short activation procedure. In this paper, it was shown that the requisite structure can be obtained by means of an electrochemical process in the operating fuel cell. This process takes place under the special conditions present in the cathode of a DMFC, namely milder oxidizing conditions and higher humidity compared to the cathode of a hydrogen fuel cell.

#### AUTHOR INFORMATION

##### Corresponding Author

\*E-mail: [a.gluesen@fz-juelich.de](mailto:a.gluesen@fz-juelich.de).

##### ORCID

Andreas Glösen: 0000-0002-5986-1759

Lin Gan: 0000-0003-3486-6016

Peter Strasser: 0000-0002-3884-436X

## Notes

The authors declare no competing financial interest.

## ACKNOWLEDGMENTS

P.P. is thankful for the support by the Bundesministerium für Bildung und Forschung (funding registration number: FK03ET6080E).

## REFERENCES

- (1) Mergel, J.; Janssen, H.; Müller, M.; Wilhelm, J.; Stolten, D. Development of Direct Methanol Fuel Cell Systems for Material Handling Applications. *J. Fuel Cell Sci. Technol.* **2012**, *9*, 031011.
- (2) Müller, M.; Kimiaie, N.; Glüsen, A.; Stolten, D. The Long Way of Achieving a Durability of 20,000 H in a DMFC System. *Adv. Sci. Technol.* **2014**, *93*, 56–60.
- (3) Müller, M.; Kimiaie, N.; Glüsen, A. Direct Methanol Fuel Cell Systems for Backup Power – Influence of the Standby Procedure on the Lifetime. *Int. J. Hydrogen Energy* **2014**, *39*, 21739–21745.
- (4) Rashidi, R.; Dincer, I.; Naterer, G. F.; Berg, P. Performance Evaluation of Direct Methanol Fuel Cells for Portable Applications. *J. Power Sources* **2009**, *187*, 509–516.
- (5) Kimiaie, N.; Wedlich, K.; Hehemann, M.; Lambert, R.; Müller, M.; Korte, C.; Stolten, D. Results of a 20 000 H Lifetime Test of a 7 kW Direct Methanol Fuel Cell (DMFC) Hybrid System - Degradation of the DMFC Stack and the Energy Storage. *Energy Environ. Sci.* **2014**, *7*, 3013–3025.
- (6) Hamnett, A. Mechanism and Electrocatalysis in the Direct Methanol Fuel Cell. *Catal. Today* **1997**, *38*, 445–457.
- (7) Rossmel, J.; Ferrin, P.; Tritsarlis, G. A.; Nilekar, A. U.; Koh, S.; Bae, S. E.; Brankovic, S. R.; Strasser, P.; Mavrikakis, M. Bifunctional Anode Catalysts for Direct Methanol Fuel Cells. *Energy Environ. Sci.* **2012**, *5*, 8335–8342.
- (8) Strasser, P. Combinatorial Optimization of Ternary Pt Alloy Catalysts for the Electrooxidation of Methanol. *J. Comb. Chem.* **2008**, *10*, 216–224.
- (9) Antolini, E.; Lopes, T.; Gonzalez, E. R. An Overview of Platinum-Based Catalysts as Methanol-Resistant Oxygen Reduction Materials for Direct Methanol Fuel Cells. *J. Alloys Compd.* **2008**, *461*, 253–262.
- (10) Singh, R. N.; Awasthi, R.; Sharma, C. S. Review: An Overview of Recent Development of Platinum-Based Cathode Materials for Direct Methanol Fuel Cells. *Int. J. Electrochem. Sci.* **2014**, *9*, 5607–5639.
- (11) Zignani, S. C.; Baglio, V.; Sebastian, D.; Rocha, T. A.; Gonzalez, E. R.; Arico, A. S. Investigation of PtNi/C as Methanol Tolerant Electrocatalyst for the Oxygen Reduction Reaction. *J. Electroanal. Chem.* **2016**, *763*, 10–17.
- (12) Wippermann, K.; Richter, B.; Klafki, K.; Mergel, J.; Zehl, G.; Dorbandt, I.; Bogdanoff, P.; Fiechter, S.; Kaytakoglu, S. Carbon Supported Ru-Se as Methanol Tolerant Catalysts for DMFC Cathodes. Part II: Preparation and Characterization of Meas. *J. Appl. Electrochem.* **2007**, *37*, 1399–1411.
- (13) Choi, B.; Nam, W.-H.; Chung, D. Y.; Park, I.-S.; Yoo, S. J.; Song, J. C.; Sung, Y.-E. Enhanced Methanol Tolerance of Highly Pd Rich Pd-Pt Cathode Electrocatalysts in Direct Methanol Fuel Cells. *Electrochim. Acta* **2015**, *164*, 235–242.
- (14) Lo Vecchio, C.; Sebastian, D.; Lazaro, M. J.; Arico, A. S.; Baglio, V. Methanol-Tolerant M-N-C Catalysts for Oxygen Reduction Reactions in Acidic Media and Their Application in Direct Methanol Fuel Cells. *Catalysts* **2018**, *8*, 650.
- (15) Piela, B.; Olson, T. S.; Atanassov, P.; Zelenay, P. Highly Methanol-Tolerant Non-Precious Metal Cathode Catalysts for Direct Methanol Fuel Cell. *Electrochim. Acta* **2010**, *55*, 7615–7621.
- (16) Lufano, F.; Baglio, V.; Staiti, P.; Antonucci, V.; Arico, A. S. Performance Analysis of Polymer Electrolyte Membranes for Direct Methanol Fuel Cells. *J. Power Sources* **2013**, *243*, 519–534.
- (17) Kreuer, K. D. On the Development of Proton Conducting Polymer Membranes for Hydrogen and Methanol Fuel Cells. *J. Membr. Sci.* **2001**, *185*, 29–39.
- (18) Glüsen, A.; Stolten, D. Membranes for Polymer Electrolyte Fuel Cells. *Chem. Ing. Tech.* **2003**, *75*, 1591–1597.
- (19) Colpan, C. O.; Ouellette, D.; Glüsen, A.; Müller, M.; Stolten, D. Reduction of Methanol Crossover in a Flowing Electrolyte-Direct Methanol Fuel Cell. *Int. J. Hydrogen Energy* **2017**, *42*, 21530–21545.
- (20) Greeley, J.; Stephens, I. E. L.; Bondarenko, A. S.; Johansson, T. P.; Hansen, H. A.; Jaramillo, T. F.; Rossmeisl, J.; Chorkendorff, I.; Nørskov, J. K. Alloys of Platinum and Early Transition Metals as Oxygen Reduction Electrocatalysts. *Nat. Chem.* **2009**, *1*, 552–556.
- (21) Stamenkovic, V. R.; Mun, B. S.; Arenz, M.; Mayrhofer, K. J. J.; Lucas, C. A.; Wang, G. F.; Ross, P. N.; Markovic, N. M. Trends in Electrocatalysis on Extended and Nanoscale Pt-Bimetallic Alloy Surfaces. *Nat. Mater.* **2007**, *6*, 241–247.
- (22) Beyhan, S.; Sahin, N. E.; Pronier, S.; Leger, J. M.; Kadirgan, F. Comparison of Oxygen Reduction Reaction on Pt/C, Pt-Sn/C, Pt-Ni/C, and Pt-Sn-Ni/C Catalysts Prepared by Bonnemant Method: A Rotating Ring Disk Electrode Study. *Electrochim. Acta* **2015**, *151*, 565–573.
- (23) Ahrenstorf, K.; Albrecht, O.; Heller, H.; Kornowski, A.; Gortitz, D.; Weller, H. Colloidal Synthesis of NixPt1-x Nanoparticles with Tuneable Composition and Size. *Small* **2007**, *3*, 271–274.
- (24) Wang, D. L.; Xin, H. L. L.; Hovden, R.; Wang, H. S.; Yu, Y. C.; Müller, D. A.; DiSalvo, F. J.; Abruna, H. D. Structurally Ordered Intermetallic Platinum-Cobalt Core-Shell Nanoparticles with Enhanced Activity and Stability as Oxygen Reduction Electrocatalysts. *Nat. Mater.* **2013**, *12*, 81–87.
- (25) Markovic, N. M.; Schmidt, T. J.; Stamenkovic, V.; Ross, P. N. Oxygen Reduction Reaction on Pt and Pt Bimetallic Surfaces: A Selective Review. *Fuel Cells* **2001**, *1*, 105–116.
- (26) Ding, L.-X.; Wang, A.-L.; Li, G.-R.; Liu, Z.-Q.; Zhao, W.-X.; Su, C.-Y.; Tong, Y.-X. Porous Pt-Ni-P Composite Nanotube Arrays: Highly Electroactive and Durable Catalysts for Methanol Electrooxidation. *J. Am. Chem. Soc.* **2012**, *134*, 5730–5733.
- (27) Gan, L.; Heggen, M.; Rudi, S.; Strasser, P. Core-Shell Compositional Fine Structures of Dealloyed PtxNi1-x Nanoparticles and Their Impact on Oxygen Reduction Catalysis. *Nano Lett.* **2012**, *12*, 5423–5430.
- (28) Cui, C. H.; Gan, L.; Li, H. H.; Yu, S. H.; Heggen, M.; Strasser, P. Octahedral PtNi Nanoparticle Catalysts: Exceptional Oxygen Reduction Activity by Tuning the Alloy Particle Surface Composition. *Nano Lett.* **2012**, *12*, 5885–5889.
- (29) Gan, L.; Heggen, M.; Cui, C. H.; Strasser, P. Thermal Facet Healing of Concave Octahedral Pt-Ni Nanoparticles Imaged in Situ at the Atomic Scale: Implications for the Rational Synthesis of Durable High-Performance ORR Electrocatalysts. *ACS Catal.* **2016**, *6*, 692–695.
- (30) Cui, C. H.; Gan, L.; Heggen, M.; Rudi, S.; Strasser, P. Compositional Segregation in Shaped Pt Alloy Nanoparticles and Their Structural Behaviour During Electrocatalysis. *Nat. Mater.* **2013**, *12*, 765–771.
- (31) Han, B.; Carlton, C. E.; Kongkanand, A.; Kukreja, R. S.; Theobald, B. R.; Gan, L.; O'Malley, R.; Strasser, P.; Wagner, F. T.; Shao-Horn, Y. Record Activity and Stability of Dealloyed Bimetallic Catalysts for Proton Exchange Membrane Fuel Cells. *Energy Environ. Sci.* **2015**, *8*, 258–266.
- (32) Zhang, J.; Mo, Y.; Vukmirovic, M. B.; Klie, R.; Sasaki, K.; Adzic, R. R. Platinum Monolayer Electrocatalysts for O<sub>2</sub> Reduction: Pt Monolayer on Pd(111) and on Carbon-Supported Pd Nanoparticles. *J. Phys. Chem. B* **2004**, *108*, 10955–10964.
- (33) Zhang, J. L.; Vukmirovic, M. B.; Xu, Y.; Mavrikakis, M.; Adzic, R. R. Controlling the Catalytic Activity of Platinum-Monolayer Electrocatalysts for Oxygen Reduction with Different Substrates. *Angew. Chem., Int. Ed.* **2005**, *44*, 2132–2135.
- (34) Adzic, R. R.; Zhang, J.; Sasaki, K.; Vukmirovic, M. B.; Shao, M.; Wang, J. X.; Nilekar, A. U.; Mavrikakis, M.; Valerio, J. A.; Uribe, F.

Platinum Monolayer Fuel Cell Electrocatalysts. *Top. Catal.* **2007**, *46*, 249–262.

(35) Stamenkovic, V. R.; Fowler, B.; Mun, B. S.; Wang, G. F.; Ross, P. N.; Lucas, C. A.; Markovic, N. M. Improved Oxygen Reduction Activity on Pt<sub>3</sub>Ni(111) Via Increased Surface Site Availability. *Science* **2007**, *315*, 493–497.

(36) Stamenkovic, V. R.; Mun, B. S.; Mayrhofer, K. J. J.; Ross, P. N.; Markovic, N. M. Effect of Surface Composition on Electronic Structure, Stability, and Electrocatalytic Properties of Pt-Transition Metal Alloys: Pt-Skin Versus Pt-Skeleton Surfaces. *J. Am. Chem. Soc.* **2006**, *128*, 8813–8819.

(37) Erlebacher, J.; Aziz, M. J.; Karma, A.; Dimitrov, N.; Sieradzki, K. Evolution of Nanoporosity in Dealloying. *Nature* **2001**, *410*, 450–453.

(38) Koh, S.; Strasser, P. Electrocatalysis on Bimetallic Surfaces: Modifying Catalytic Reactivity for Oxygen Reduction by Voltammetric Surface Dealloying. *J. Am. Chem. Soc.* **2007**, *129*, 12624–12625.

(39) Strasser, P.; Koh, S.; Anniyev, T.; Greeley, J.; More, K.; Yu, C. F.; Liu, Z. C.; Kaya, S.; Nordlund, D.; Ogasawara, H.; Toney, M. F.; Nilsson, A. Lattice-Strain Control of the Activity in Dealloyed Core-Shell Fuel Cell Catalysts. *Nat. Chem.* **2010**, *2*, 454–460.

(40) Wang, C.; Chi, M.; Wang, G.; van der Vliet, D.; Li, D.; More, K.; Wang, H. H.; Schlueter, J. A.; Markovic, N. M.; Stamenkovic, V. R. Correlation between Surface Chemistry and Electrocatalytic Properties of Monodisperse Pt<sub>x</sub>Ni<sub>1-x</sub> Nanoparticles. *Adv. Funct. Mater.* **2011**, *21*, 147–152.

(41) Sasaki, K.; Naohara, H.; Cai, Y.; Choi, Y. M.; Liu, P.; Vukmirovic, M. B.; Wang, J. X.; Adzic, R. R. Core-Protected Platinum Monolayer Shell High-Stability Electrocatalysts for Fuel-Cell Cathodes. *Angew. Chem., Int. Ed.* **2010**, *49*, 8602–8607.

(42) Dohle, H.; Mergel, J.; Stolten, D. Heat and Power Management of a Direct-Methanol-Fuel-Cell (DMFC) System. *J. Power Sources* **2002**, *111*, 268–282.

(43) Piela, P.; Fields, R.; Zelenay, P. Electrochemical Impedance Spectroscopy for Direct Methanol Fuel Cell Diagnostics. *J. Electrochem. Soc.* **2006**, *153*, A1902–A1913.

(44) Eickes, C.; Piela, P.; Davey, J.; Zelenay, P. Recoverable Cathode Performance Loss in Direct Methanol Fuel Cells. *J. Electrochem. Soc.* **2006**, *153*, A171–A178.

(45) Sgroi, M.; Zedde, F.; Barbera, O.; Stassi, A.; Sebastián, D.; Lufitano, F.; Baglio, V.; Aricò, A.; Bonde, J.; Schuster, M. Cost Analysis of Direct Methanol Fuel Cell Stacks for Mass Production. *Energies* **2016**, *9*, 1008.

(46) Zago, M.; Bisello, A.; Baricci, A.; Rabissi, C.; Brightman, E.; Hinds, G.; Casalegno, A. On the Actual Cathode Mixed Potential in Direct Methanol Fuel Cells. *J. Power Sources* **2016**, *325*, 714–722.

(47) Kulikovskiy, A. A.; Schmitz, H.; Wippermann, K.; Mergel, J.; Fricke, B.; Sanders, T.; Sauer, D. U. Bifunctional Activation of a Direct Methanol Fuel Cell. *J. Power Sources* **2007**, *173*, 420–423.

(48) Glösen, A.; Müller, M.; Stolten, D. The Effect of Nafion Content on DMFC Electrode Characteristics. *ECS Trans.* **2013**, *58*, 1023–1029.

(49) Momma, K.; Izumi, F. Vesta 3 for Three-Dimensional Visualization of Crystal, Volumetric and Morphology Data. *J. Appl. Crystallogr.* **2011**, *44*, 1272–1276.